Unconventional gap dependence of high-order harmonic generation in the extremely strong light-matter-coupling regime

Akira Kofuji* and Robert Peters†
Department of Physics, Kyoto University, Kyoto 606-8502, Japan

(Received 28 April 2023; accepted 4 August 2023; published 25 August 2023)

High-order harmonic generation (HHG) is one of the most commonly studied nonlinear optical phenomena, originating in the ultrafast dynamics of electrons in atomic gases and semiconductors. It has attracted much attention because of its nonperturbative nature and potential for future attosecond laser pulse sources. On the theory side, a semiclassical picture based on tunneling ionization of electrons is successfully used in explaining key characteristics of the HHG. This model assumes that electric fields nonperturbatively excite electrons beyond the ionization potential or the band gap. Thus, intuitively, a larger gap should lead to an exponentially smaller HHG emission. Despite this intuition, the HHG in the Mott insulator Ca_2RuO_4 has shown an unconventional exponential increase with respect to the gap width. This experiment implies effects beyond the semiclassical theory. However, most theoretical works have focused on the dependence of the HHG on external control parameters, and the gap dependence of the HHG is poorly understood even in noninteracting systems. Thus, it is essential to clarify the gap dependence of the HHG in a fully quantum mechanical approach. Here, we analyze numerically exactly the gap dependence of the HHG in two-level systems. We find an increase in the strength of the HHG when the Rabi frequency is large compared to the gap width. Furthermore, the relaxation and scattering of electrons increase the visibility of this gap dependence. Finally, we find that the enhancement rate follows a universal scaling law regardless of the driving frequency. The existence of this gap dependence in two-level systems suggests that this unconventional gap dependence is a universal behavior that can be found not only in Mott insulators but also in atomic gases and semiconductors.

DOI: 10.1103/PhysRevA.108.023521

I. INTRODUCTION

Decades of progress in strong laser light technologies have made it possible to probe and control the ultrafast dynamics of electrons in materials. One of the most commonly studied optical phenomena in the field of strong laser light is the high-order harmonic generation (HHG) in atomic gases [1–3] and solids [4,5], where photons with multiples of the driving photon energy are emitted, and the spectrum consists of a characteristic plateau and cutoff energy. HHG has attracted much attention not only because it is a nonperturbative phenomenon with great potential for future attosecond light sources but also because it can be a new all-optical probe for states of matter, i.e., high-order harmonic spectroscopy [6–26]. For example, HHG is now utilized for probing molecular orbitals [6], band structures [12], the Berry curvature of materials [18,24], topological phase transitions [23], and Majorana fermions [26]. Recently, various types of HHG, unique to strongly correlated electron systems, have also been intensively studied [27–42], opening possibilities to detect ultrafast light-induced phase transitions [28], quantum phase transitions [36], and transitions from the strange metal phase to the pseudogap phase [37].

Almost all of these previous studies can be understood based on the well-known semiclassical three-step model [43,44], which consists of (i) tunnel ionization of electrons trapped in some potential, (ii) forced oscillatory motion, and (iii) recombination of electrons in the potential. This simple yet powerful model successfully explains the essential characteristics of the HHG, i.e., the plateau and the cutoff energy, and has been extended to solids [45]. However, the nonlinearity of the band velocity in solids enriches the HHG by evoking intraband processes, which are also closely intertwined with interband processes. Moreover, because of the periodicity of solids, the recombination is not restricted to the original lattice site, where the electron is excited, and this might enable real-space imaging of lattice potentials [46]. A general feature of the tunnel ionization process in the three-step model of atomic gases and solids is that the tunneling amplitude becomes exponentially small when the driving frequency is sufficiently smaller than the gap [47–53]. Thus, the three-step model leads us to the naive expectation that the HHG emission should also become exponentially small when the gap width becomes large.

Recently, an unconventional HHG which contradicts this intuition has been experimentally observed in the Mott insulator Ca_2RuO_4 [39]. Utilizing the temperature dependence of the Mott gap of this material, the dependence of the HHG on the excitation gap has been investigated, and it has been shown that the HHG grows exponentially as the gap width increases. More surprisingly, the gap dependence obeys an

*kofuji.akira.46c@st.kyoto-u.ac.jp
†peters@scphys.kyoto-u.ac.jp

empirical and universal scaling law regardless of the driving frequency. While such a strange gap dependence has been observed in experiments, most theoretical studies have focused on the dependence of the HHG on external control parameters, such as the ellipticity, strength, and carrier-envelope phase of the incident laser pulse [54,55]. Recently, Murakami *et al.* [56] have studied the unconventional temperature (gap) dependence of the HHG by analyzing the laser-driven Hubbard model with nonequilibrium dynamical mean-field theory, suggesting a relation between the unconventional gap dependence and doublon scattering. Murakami and Schüler [57] have also studied the gap dependence of the HHG in gapped graphene, where they have found that the modification of the intraband dipole via interband transitions leads to a nonmonotonic gap dependence of the HHG. While these studies show that the HHG can have an unconventional gap dependence in correlated systems and gapped graphene, the gap dependence of the HHG in noninteracting systems is actually not well understood. It remains unclear to what extent the unconventional gap dependence is due to correlations and whether it can also be observed in uncorrelated systems. Furthermore, understanding the gap dependence of the HHG can open a new path to realize a stronger HHG emission by tuning the excitation gap of materials and new high-order harmonic spectroscopic methods through the gap dependence of the HHG.

We here demonstrate that an unconventional gap dependence of the HHG can be observed even in uncorrelated models. For this purpose, we study the HHG in a two-level system. Two-level systems are very simplified models that do not include intraband current and multiband effects, which occur in realistic solid-state systems. However, two-level systems still share various aspects of the HHG in atomic gases and solids [58–62]. The advantage of these simplified models is that we can reduce the numerical cost significantly. Thus, we can investigate the HHG in a fully quantum mechanical approach and numerically exactly in a wide range of parameters, such as the Rabi frequency, the relaxation time, and the excitation gap. Based on this two-level system, we first analyze the gap dependence of the HHG varying the Rabi frequency. We observe an increase in the HHG with increasing gap width when the Rabi frequency is large compared to the gap. In contrast, the HHG decreases exponentially when the gap is large. To investigate the origin of this gap dependence, we consider the effects of relaxation processes on the HHG and calculate the time-resolved spectrum of the HHG. We see that relaxation is not necessary for the appearance of an unconventional gap dependence. Finally, we study the enhancement ratio at each emission energy and see that it obeys a universal behavior regardless of the incidental frequency, which is also observed in the experiment [39]. From the above analysis, we expect that this unconventional gap dependence of the HHG, as observed in the experiment, is a universal characteristic not only found in Mott insulators but also in atomic gases and semiconductors.

The remainder of this paper is structured as follows. Section II introduces the two-level system driven by an electric laser pulse. In Sec. III, we analyze the gap dependence of the HHG and the effects of relaxation processes. Finally, we calculate the enhancement ratio of the emission energy and show its universal behavior. Finally, we conclude the paper in Sec. IV. Furthermore, we show an analysis of the HHG in semiconductors based on semiconductor Bloch equations in the Appendix.

II. MODEL AND METHODS

First, we explain the Hamiltonian of the two-level system. In this paper, we use the following units: $e = \hbar = d = 1$, which correspond to the elementary charge, Planck's constant, and the transition dipole moment of the system. We also set $\hbar\omega_u = 1$ eV $= 1$ as a unit for energy. Then, the Hamiltonian can be written as

$$\hat{H}(t) = \hat{H}_0 + \hat{H}_{\rm ext} = \begin{bmatrix} -\Delta/2 & -\Omega(t) \\ -\Omega(t) & \Delta/2 \end{bmatrix}. \tag{1}$$

$\hat{H}_0$ is the original Hamiltonian of the two-level system, which corresponds to the diagonal part of $\hat{H}$. $\hat{H}_{\rm ext}(t)$ is the contribution from the external electric field, which corresponds to the off-diagonal part of $\hat{H}$. Δ represents the gap of the system, and $\Omega(t)$ depends on the strength and the shape of the electric field.

To take relaxation processes into account, we use the von Neuman equation, which is more suitable for calculating the time evolution of this system. Calculating the commutator of the Hamiltonian, Eq. (1), and the density matrix of the system, $\hat{\rho}$, and adding relaxation terms, we arrive at the following equations of motion [58]:

$$\dot{x} = 2i\Omega(t)(y - y^*) - \gamma_{\rm L}(x - 1), \tag{2}$$

$$\dot{y} = -(i\Delta + \gamma_{\rm T})y + i\Omega(t)x. \tag{3}$$

$x = \rho_{11} - \rho_{22}$ is the population difference of the levels in the system, and $y = \rho_{21}$ measures the coherence between both levels. $\gamma_{\rm L}$ is the longitudinal relaxation rate, which induces the relaxation from the upper level to the lower level, and $\gamma_{\rm T}$ is the transverse relaxation rate, which induces decoherence between both levels. The origin of these relaxation terms can be traced back to spontaneous emission, interatomic interactions, electron-electron interactions, and electron-phonon interactions. In this paper, it is not our primary purpose to study how these relaxation terms appear from microscopic interactions. Thus, we include these relaxation processes just phenomenologically. (For details, see Ref. [63].)

In two-level systems, the origin of the HHG is a fast oscillation of the polarization of the system. To obtain the spectrum of the HHG, first, we numerically calculate the time dependence of the density matrix ρ of the system and obtain the time-dependent expectation value of the position operator, corresponding to the polarization given as

$$p(t) = {\rm Tr}[\hat{\rho}(t)\hat{x}] = y + y^*. \tag{4}$$

Then, by calculating the Fourier transform of the polarization, we obtain the spectrum of the HHG. We note that the transition dipole moment is assumed to be constant here. The external field is modulated by a Gaussian amplitude and is written as

$$\Omega(t) = \Omega_0 \cos(\omega_0 t) e^{-t^2/\tau^2}. \tag{5}$$

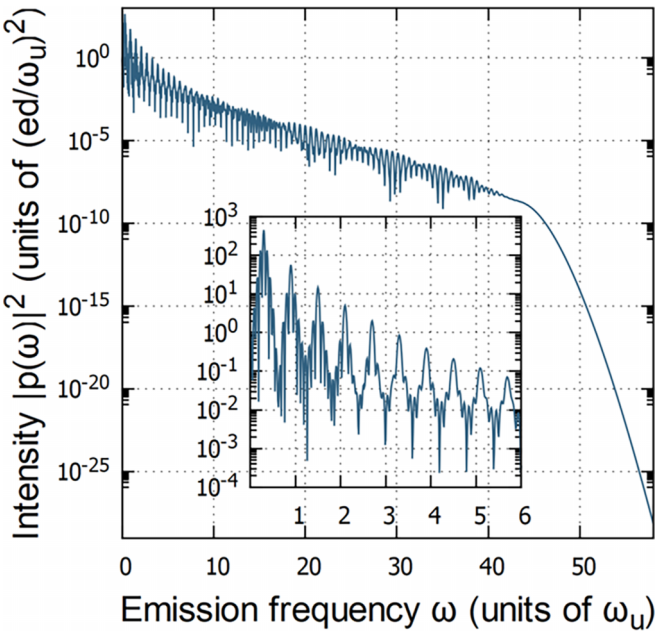

FIG. 1. A typical example of an HHG spectrum. The inset shows the enlarged view of the spectrum for low frequencies. The parameters are $\Delta = 2.1$, $\Omega_0 = 22.7$, $\gamma_L = 2.0$, $\gamma_T = 1.0$, $\tau = 8.5\pi$, and $\omega_0 = 0.3$. The vertical axis is log scale.

Ω_0 is the Rabi frequency, which is the product of the strength of the electric field and the transition dipole moment. ω_0 is the frequency of the incidental light.

The HHG in a two-level system has common characteristics with the HHG in atomic potentials and solids. We here briefly review the mechanism of the HHG in two-level systems following Ref. [61]. For the sake of simplicity, we ignore relaxation processes and analyze the Hamiltonian in Eq. (1). We note that the "adiabatic" basis is more convenient for understanding the origin of the HHG. The adiabatic basis diagonalizes the time-dependent Hamiltonian $\hat{H}(t)$ at each instant of time. This can be done by the following unitary operator,

$$\hat{U}(t) = \begin{bmatrix} \cos(\chi(t)) & \sin(\chi(t)) \\ -\sin(\chi(t)) & \cos(\chi(t)) \end{bmatrix}, \tag{6}$$

where $\chi(t) = -\frac{1}{2}\tan^{-1}(\frac{2\Omega(t)}{\Delta})$. In this basis, the time evolution of the system is described by the following Hamiltonian,

$$\hat{H}'(t) = \hat{U}^\dagger(t)\hat{H}(t)\hat{U}(t) + i\frac{\partial \hat{U}^\dagger}{\partial t}\hat{U}(t) = \begin{bmatrix} \varepsilon_-(t) & -i\dot{\chi} \\ i\dot{\chi} & \varepsilon_+(t) \end{bmatrix}, \tag{7}$$

where $\varepsilon_\pm = \pm\frac{1}{2}\sqrt{\Delta^2 + 4\Omega^2(t)}$ are the "eigenenergies" at each instant, and $i\dot{\chi}$ induces a nonadiabatic transition between the "energy" levels, which is given as $\dot{\chi} = -\frac{\dot{\Omega}/\Delta}{1+(2\Omega(t)/\Delta)^2}$. Transitions between both states can easily occur near the nodes of the pulse, where $\Omega(t) = 0$. On the other hand, the states evolve adiabatically near the antinodes of the pulse, where $\dot{\Omega} = 0$ so that $\dot{\chi} = 0$. Thus, in intervals of time with small electric fields, the electrons in the lower "energy" level are excited to the upper level, then perform an adiabatic time evolution generating ultrafast oscillations of the polarization, and finally return to the lower level. This process is analogous to the three-step model in atomic gases and solids. Furthermore, in semiconductors, the description of the system is identical to that of the two-level system under special conditions, such as low doping and identical effective masses in the valence and conduction bands [61,64,65]. Therefore, the HHG in two-level systems can capture the general characteristics of the HHG in various systems.

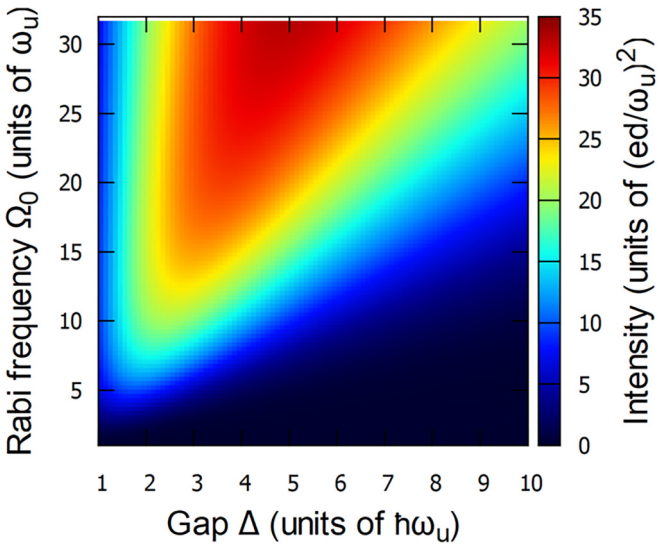

FIG. 2. Gap and Rabi frequency dependence of the 5th harmonics ($\omega = 5\omega_0$).

A typical example of an HHG spectrum, calculated in the two-level system, is shown in Fig. 1. The spectrum shows the characteristic of the HHG, i.e., the plateau, at which the intensity of the spectrum stays constant or only decreases slightly with increasing harmonic order, and the cutoff at high frequencies, above which the intensity decreases quickly. We note that throughout the paper the incidental frequency is much smaller than the gap energy. Thus, the system is off-resonant. We consider the case in which the tunneling ionization is dominant compared to multiphoton excitations.

III. RESULTS

A. Unconventional gap dependence

First, we analyze the strength of the HHG depending on the gap width Δ and the Rabi frequency Ω_0. In this subsection, τ, ω_0, γ_L, and γ_T are fixed as $\tau = 8.5\pi$, $\omega_0 = 0.3$, and $\gamma_L = 2\gamma_T = 2.0$, and we vary Δ and Ω_0. In Fig. 2, we show the intensity of the $5\omega_0$ harmonics for various gap widths and Rabi frequencies. For sufficiently large values of the Rabi frequency compared to the gap width, i.e., in the upper left region of Fig. 2, the intensity of the HHG grows as the gap increases. The intensity takes a maximum at approximately $\Omega_0/\Delta \sim 6$ and decreases for larger gap widths. To confirm this behavior, we show the intensity for $\Omega_0 = 22.7$ over the gap width in Fig. 3. This figure reveals that the intensity increases until the gap reaches some threshold value and then decreases exponentially. This nonmonotonic behavior suggests that the naive intuition that larger gaps result in a

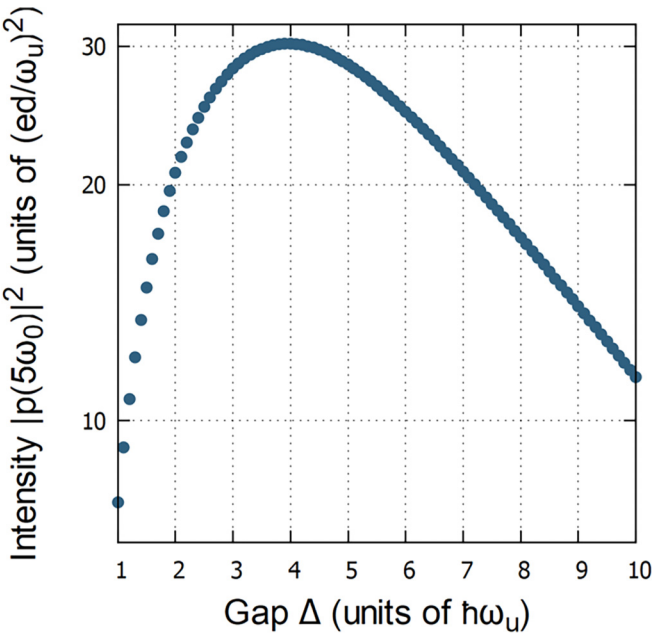

FIG. 3. Gap dependence of the 5th harmonics for $\Omega_0 = 22.7$. The vertical axis is log scale.

smaller HHG intensity is not true for large values of the Rabi frequency. We note that the $5\omega_0$ harmonics represents a typical harmonic order. Indeed, Fig. 2 looks very similar for all odd harmonics between the 3rd and the 23rd harmonics (using the current parameters). Thus, we use the $5\omega_0$ harmonics in the rest of this paper.

To understand the enhancement of the HHG for small gap widths better, we next analyze the time dependence of the HHG. We first show in Fig. 4 the time evolution of $x(t)$ and $\mathrm{Re}[y(t)]$ for three different parameters using $\Omega_0 = 22.7$, corresponding to the three different regimes, i.e., (a) the regime where the strength of the HHG increases with increasing gap width at $\Delta = 1.5$, (b) the regime where the strength of the HHG is near the maximum at $\Delta = 4$, and (c) the regime where the strength of the HHG decreases with increasing gap width at $\Delta = 9$. As described above, $x(t)$ is the occupation difference between both levels and the real part of $y(t)$ corresponds to the polarization.

In all regimes, $x(t)$ decreases at small times; electrons are excited to the other level. However, we see that $x(t)$ decreases faster for small gaps. This also results in faster growth of the polarization at small times if the gap is small, which is demonstrated by a horizontal arrow indicating the value of the peak of $y(t)$ around $t \sim -50$ in each figure for clarity. This corresponds to the fact that electrons are easily excited when the gap is small. We can determine the time at which a high harmonic is generated by multiplying the polarization with a Gaussian window function before Fourier transform. This results in an HHG spectrum, which depends on time through the window function as

$$p(\omega, t_p) = \int_{-\infty}^{\infty} dt\, p(t) W(t, t_p) e^{i\omega t}, \tag{8}$$

$$W(t, t_p) = \frac{1}{\sqrt{2\pi\sigma^2}} e^{-\frac{(t-t_p)^2}{2\sigma^2}}. \tag{9}$$

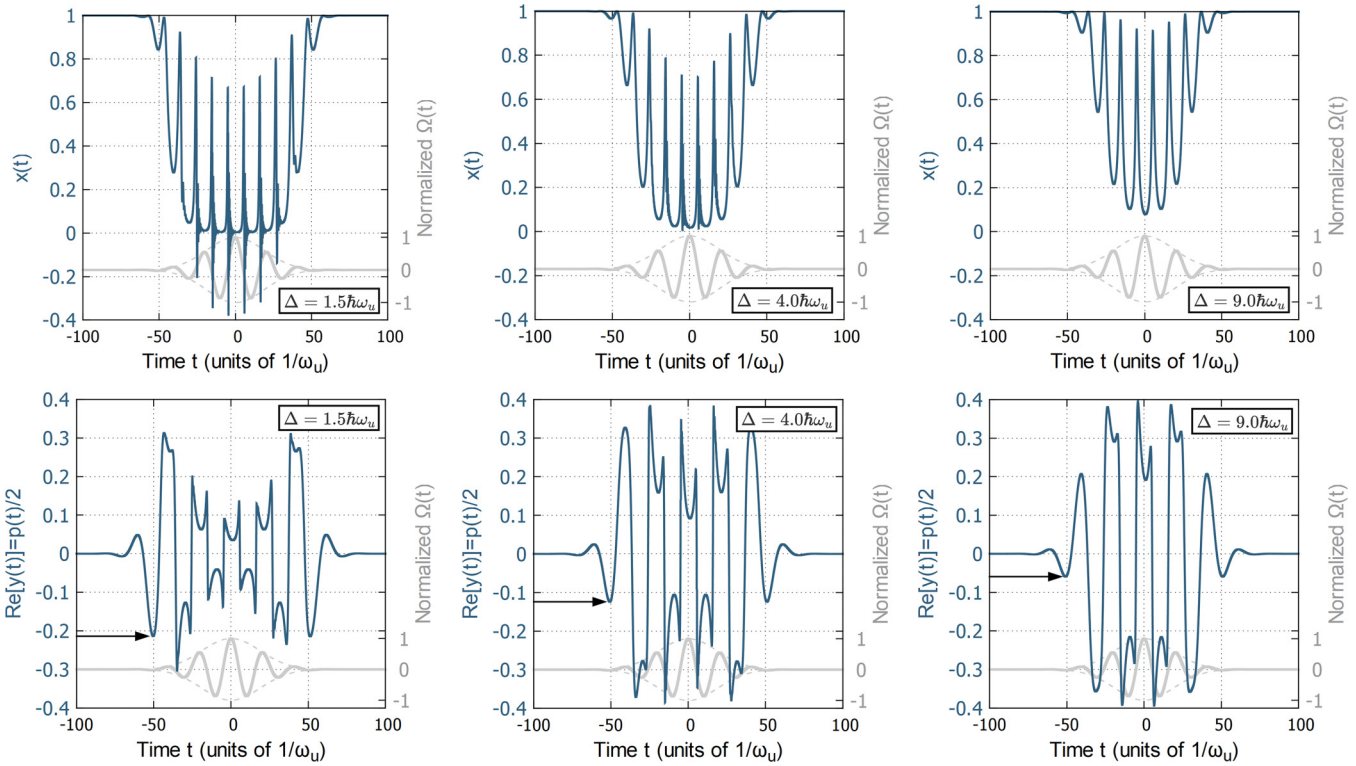

FIG. 4. Time-resolved $x(t)$ and $\mathrm{Re}[y(t)]$ for three different regimes, small gap (left panels), an intermediate gap where the $5\omega_0$ HHG is maximal (middle panels), and a large gap (right panels). The horizontal arrows in the panels of $\mathrm{Re}[y(t)]$ indicate the value of the peak of $y(t)$ around $t \sim -50$. The pulse shape of the external field is also plotted in each figure in gray. The Rabi frequency is $\Omega_0 = 22.7$.

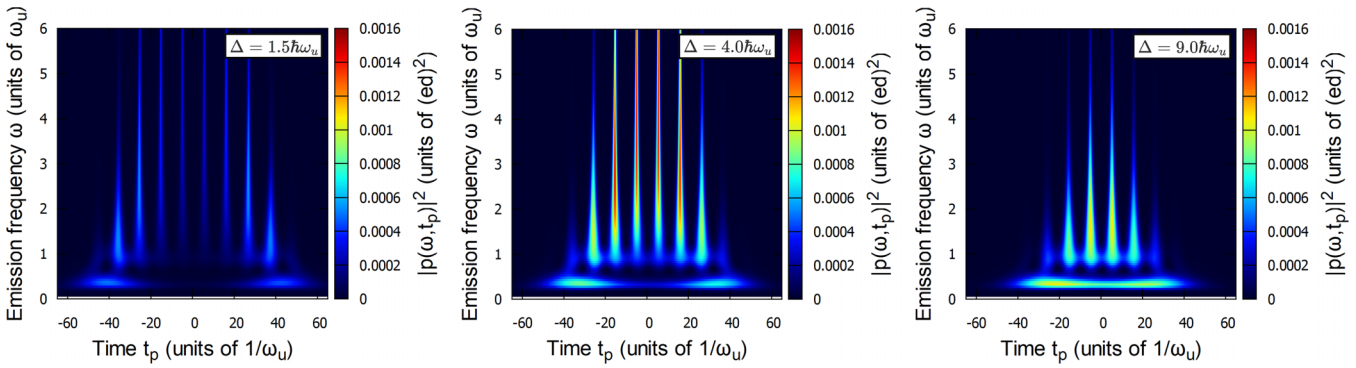

FIG. 5. Time-resolved spectrum of HHG for three different gaps (left panel: $\Delta = 1.5$; center panel: $\Delta = 4.0$; right panel: $\Delta = 9.0$). The Rabi frequency is $\Omega_0 = 22.7$.

The width of the window function used here is $\sigma = 3.5$. In Fig. 5, we show the time-resolved HHG spectrum for the same parameters as in Fig. 4. This figure shows that a reasonably strong HHG is created already at $t = -40$ for $\Delta = 1.5$, while the HHG spectrum for $\Delta = 4$ and $\Delta = 9$ is very small at this time. This HHG can be seen in the polarization as an additional dip (inside the maximum) for $\Delta = 1.5$ at $t = -40$, which is absent for $\Delta = 4$ and $\Delta = 9$. Thus, large gaps generally slow down the process of exciting electrons and the generation of high harmonics in the polarization at small times.

On the other hand, the fast decrease of $x(t)$ at small times due to a large Rabi frequency and a small gap width leads to an extended period in which $x(t)$ is small (besides a periodic spike). This results in a saturation of polarization because a finite population difference $x(t)$ is essential for the buildup of polarization [see Eq. (2)]. Finally, the magnitude of the polarization even decreases towards the center of the pulse, $t = 0$, for $\Delta = 1.5$, as can be seen in Fig. 4. As a consequence, the contribution to the HHG from the center of the pulse becomes weak. Thus, we can say that for $\Delta = 1.5$ the system is too strongly excited, which results in a situation where the HHG is only generated at the beginning and the end of the pulse but not over an extended period in the center of the pulse.

For $\Delta = 4$ in Fig. 4, we see that the magnitude of the polarization quickly reaches a large value and remains large during the whole pulse. Although the generation of the HHG starts at a time later than that for $\Delta = 1.5$, the HHG is generated over a longer time period and especially around $t = 0$. For $\Delta = 9$, the excitations of a large number of electrons, the buildup of a large polarization, and the generation of HHG take a longer time. A large HHG is only generated around the center of the pulse at $t = 0$.

We conclude here that these three regimes not only have a different HHG dependence on the gap width but can also be distinguished from their time-dependent polarization $y(t)$. Decreasing Ω_0/Δ, we see that the dominant contribution gradually moves from the start or the end to the center of the pulse. In the region where the gap dependence shows a conventional exponential decrease, the dominant contribution comes from the center of the pulse. On the other hand, in the region where the HHG grows with an increasing gap, the dominant contribution originates from the start or the end of the pulse. This implies that the origin of the unconventional gap dependence is a very strong light-matter coupling that results in the saturation of the polarization before the center of the pulse, and, thus, the contributions from the center of the pulse become weak.

B. Effects of relaxation on the gap dependence

Next, we study the effect of relaxation on the HHG. In this subsection, τ and ω_0 are fixed as $\tau = 8.5\pi$ and $\omega_0 = 0.3$, and we vary Δ, Ω_0, γ_L, and γ_T. Relaxation processes are common in various systems. They originate from interatomic interactions in atomic gases and the electron-electron interactions in solids. For example, the spin-charge coupling in Mott insulators generates a transverse relaxation term, which physically corresponds to the dephasing of doublon-holon pairs [56]. Therefore, it is important to clarify the effects of relaxation processes on the HHG, in particular, because in the strongly correlated materials, as in the Mott insulator Ca_2RuO_4, electron-electron interactions and relaxation processes can be large. In Fig. 6, we show the intensity of the $5\omega_0$ harmonics over the gap width and the strength of the Rabi frequency for three values of the relaxation rate, $\gamma_L = 2\gamma_T = 0.001$, 0.03, and 0.1. We note that the range of the gap dependence is limited to the region $\Delta \geqslant 2.0$ to avoid the effect of a multiphoton resonance at $\Delta = 5\omega_0$ so that we can understand the unconventional gap dependence more clearly.

In Fig. 6, we see that while the HHG spectrum is smooth for large relaxation rates, small relaxation rates lead to a fine structure inside the spectrum. However, these figures also show that, regardless of the value of the relaxation rate, the qualitative structure of the HHG spectrum and the unconventional gap dependence remain. Thus, when the Rabi frequency is sufficiently large compared to the gap width, the HHG grows as the gap increases, regardless of the value of the relaxation rate. Thus, we conclude that relaxation processes are not essential for the observation of the unconventional gap dependence in the HHG. However, relaxation processes help us observe it by hiding the fine structure.

C. Emission energy dependence of enhancement rate of HHG

Finally, we show in Fig. 7 the enhancement ratio for small gap widths, $|p(\omega; \Delta = 1.5)|^2/|p(\omega; \Delta = 1.0)|^2$, over the

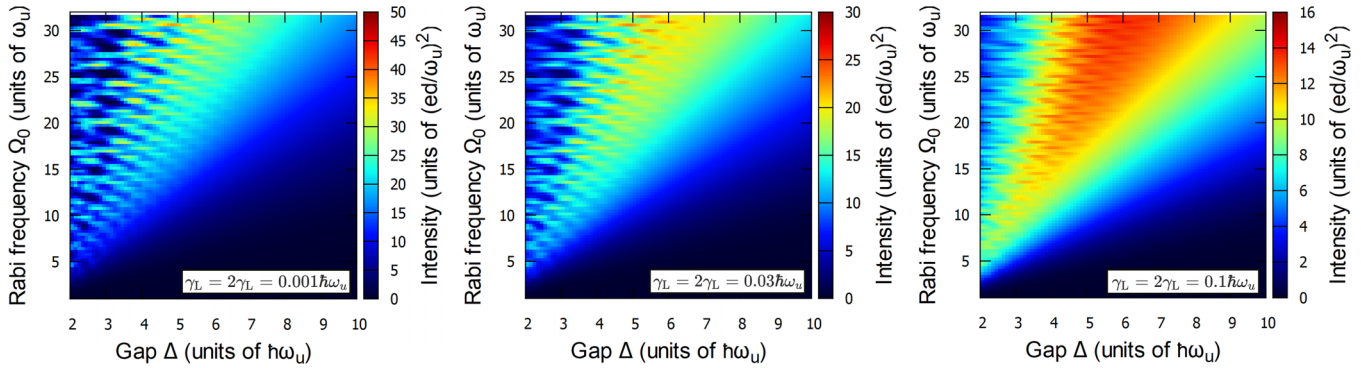

FIG. 6. Gap and Rabi frequency dependence of the 5th harmonics ($\omega = 5\omega_0$) for three different relaxation rates (left panel: γ_L=2γ_T=0.001; center panel: $\gamma_L = 2\gamma_T = 0.03$; and right panel: $\gamma_L = 2\gamma_T = 0.1$)

emission frequency for different incidental frequencies ω_0. The incidental frequency is varied in the range $\omega_0 = 0.3 \sim 0.9$. Thus, this figure includes different high harmonics depending on ω and ω_0. This figure shows that the enhancement ratio obeys a universal behavior regardless of the incidental frequency until $\omega \sim 4.0$. It also shows that the enhancement is larger for larger emission energy. Furthermore, especially around $\omega_{\text{emit}} = 1.0 \sim 3.0$, we can see that the enhancement ratio shows a power-law dependence with respect to the emission energy. This behavior is consistent with the experimental observation of an unconventional scaling law in Ca_2RuO_4 [39].

We note that, for frequencies $\omega = 4 \sim 7$, it seems that the scaling law breaks down. The frequency at which the scaling law breaks down is related to the definition of the enhancement ratio and is parameter dependent. Here, we compare the HHG intensity at $\Delta = 1.5$ and $\Delta = 1.0$ in the enhancement ratio. However, if we choose different (larger) gaps, e.g., $\Delta = 2.0$ and $\Delta = 1.5$, the scaling law in the enhancement ratio holds until higher emission frequencies. Furthermore, we note that a scaling behavior can only be observed for parameters inside the regime where the unconventional gap dependence appears, and here we have chosen $\Delta = 1.5$ and $\Delta = 1.0$ to consider a region well inside this regime. This behavior is also supported by considering the enhancement ratio in semiconductors, shown in the Appendix.

Moreover, we note that the behavior for $\omega_0 = 0.3$ deviates from the other incidental frequencies. This can be understood as an effect of the pulse duration. In the experiment on Ca_2RuO_4, the pulse duration and the incidental frequency is 100 fs and 0.26 eV (0.19 eV), respectively, which corresponds to $\omega_0\tau \sim 39.5(28.9)$. In our parameters, the product of the pulse duration and the incidental frequency is $\omega_0\tau \sim 8.0$, which is smaller than that in the experiment. As shown in Fig. 7, as the incidental frequency becomes large, i.e., as the pulse contains more cycles, the enhancement ratio converges to a single curve even in the region $\omega = 4 \sim 7$. This trend also exists in the case of semiconductors, as shown in the Appendix.

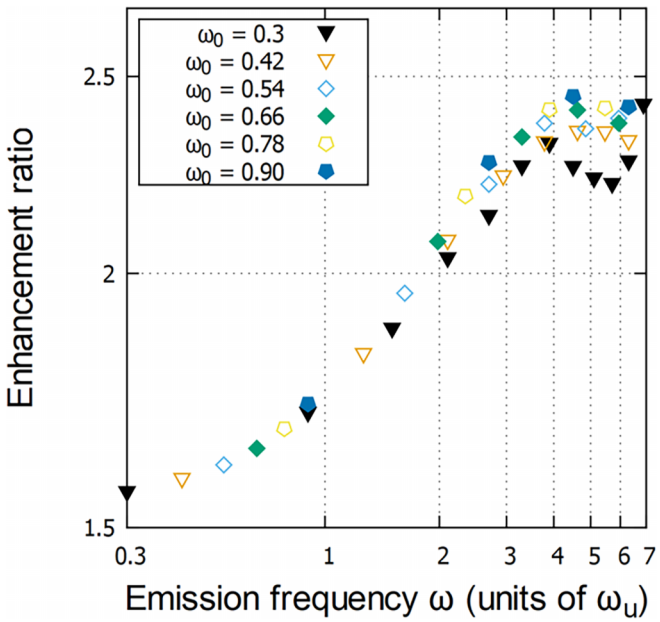

FIG. 7. Emission energy dependence of the enhancement ratio $|p(\omega;\Delta = 1.5)|^2/|p(\omega;\Delta = 1.0)|^2$ of HHG. The Rabi frequency is $\Omega_0 = 22.7$. Both of the axes are log scale.

IV. CONCLUSION

In this paper, we have demonstrated that the HHG is enhanced as the gap width increases if the Rabi frequency is sufficiently large compared to the excitation gap. This suggests that the unconventional gap dependence, experimentally observed in Ca_2RuO_4, originates in significantly strong light-matter coupling. We note that, in Mott insulators, large nonlinear optical responses have been observed, which also suggests a strong light-matter coupling in Mott-insulating systems [66–69]. Our analysis has revealed that the unconventional gap dependence is related to the saturation and even decrease in polarization towards the center of the pulse when the light-matter coupling is too strong. Thus, in the regime where the HHG is enhanced by increasing the gap width, the dominant HHG contributions appear at the start and the end of the pulse. Increasing the gap width in this regime, we find that the time when the dominant contribution appears moves towards the center of the pulse. The enhancement can thus be understood as an increase in the HHG at the center of the pulse. On the other hand, a conventional gap dependence is observed when the dominant contribution to

the HHG appears only at the center of the peak. We note that time-resolved high-order harmonic spectroscopy, utilizing the pump-probe method [70], might be able to observe this signature in Ca_2RuO_4.

Furthermore, we have shown that relaxation processes are unnecessary to induce this gap dependence of the HHG. However, it is easier to observe such a gap dependence in systems with strong relaxation because the relaxation smears fine structures in the dependence of the HHG strength on the gap width. Finally, we have investigated the enhancement of the emission energy depending on the incidental frequency. We have found a universal behavior demonstrating that the HHG increases faster for larger emission energy, which is also confirmed in semiconductors in the Appendix. This behavior is consistent with observations in Ca_2RuO_4.

ACKNOWLEDGMENTS

We thank Kento Uchida, Koki Shinada, and Yasushi Shinohara for their insightful discussions. R.P. is supported by JSPS KAKENHI Grant No. JP23K03300. This work was supported by JST, the establishment of university fellowships towards the creation of science and technology innovation, and Grant No. JPMJFS2123. Parts of the numerical simulations in this work were done using the facilities of the Supercomputer Center at the Institute for Solid State Physics, University of Tokyo.

APPENDIX: CALCULATIONS IN SEMICONDUCTORS

In this Appendix, we calculate the gap dependence of the HHG in semiconductors and confirm that the results in the main text are not restricted to two-level systems. Here, we use the following units: $e = \hbar = a = 1$, which correspond to the elementary charge, Planck's constant, and the lattice constant of the system. We also set $\hbar\omega_u = 1\ \mathrm{eV} = 1$ as a unit for energy. In this Appendix, we use the theoretical model suggested by Tamaya et *al.* [71], which can describe the parameter region where the Rabi frequency is larger than the gap width. The Hamiltonian is

$$\begin{aligned} H = &\sum_{\boldsymbol{k}} \left(E^e_{\boldsymbol{k}}\alpha^\dagger_{\boldsymbol{k}}\alpha_{\boldsymbol{k}} + E^h_{\boldsymbol{k}}\beta^\dagger_{-\boldsymbol{k}}\beta_{-\boldsymbol{k}}\right) \\ &+ \Omega(t)\sum_{\boldsymbol{k}} \cos\theta_{\boldsymbol{k}}(\alpha^\dagger_{\boldsymbol{k}}\alpha_{\boldsymbol{k}} + \beta^\dagger_{-\boldsymbol{k}}\beta_{-\boldsymbol{k}} - 1) \\ &+ i\Omega(t)\sum_{\boldsymbol{k}} \sin\theta_{\boldsymbol{k}}(\alpha^\dagger_{\boldsymbol{k}}\beta^\dagger_{-\boldsymbol{k}} - \beta_{-\boldsymbol{k}}\alpha_{-\boldsymbol{k}}). \end{aligned} \tag{A1}$$

$E^e_{\boldsymbol{k}}$ and $E^h_{\boldsymbol{k}}$ are the energy bands of the electrons and holes, $\alpha^\dagger_{\boldsymbol{k}}$ and $\alpha_{\boldsymbol{k}}$ are the creation and annihilation operators of the electrons with wave number $\boldsymbol{k}$, $\beta^\dagger_{-\boldsymbol{k}}$ and $\beta_{-\boldsymbol{k}}$ are the creation and annihilation operators of the holes with wave number $-\boldsymbol{k}$, $\theta_{\boldsymbol{k}}$ is the angle describing the wave vector $\boldsymbol{k}$ in the momentum space, and $\Omega(t)$ is the light-matter coupling. The second term corresponds to a temporal deformation of the band structure by the external field, and the third term describes an interband transition. For the detailed theoretical derivation, we refer to the original paper by Tamaya et *al.* [71]. Equations of motion

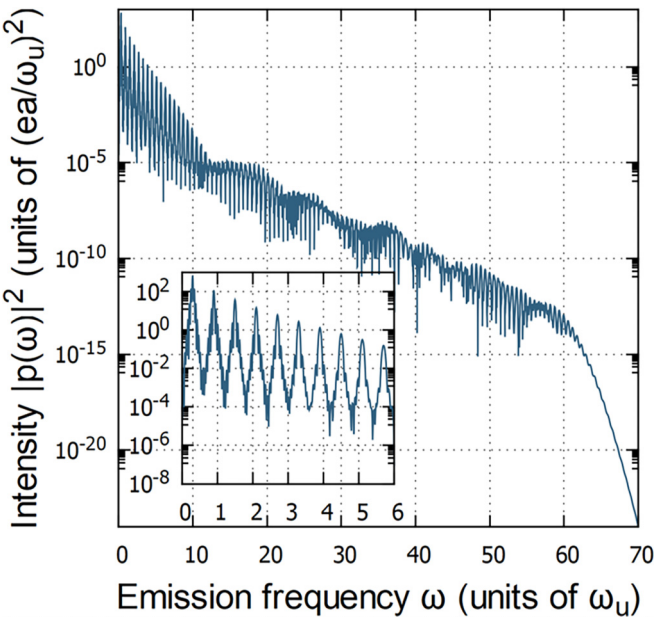

FIG. 8. A typical example of an HHG spectrum in semiconductors. The inset shows the enlarged view of the spectrum for low frequencies. The parameters are $\Delta = 2.0$, $\Omega_0 = 27.0$, and $\omega_0 = 0.3$. The vertical axis is logarithmic.

for the distribution of the electrons $f^e_{\boldsymbol{k}} = \langle\alpha^\dagger_{\boldsymbol{k}}\alpha_{\boldsymbol{k}}\rangle$, the holes $f^h_{\boldsymbol{k}} = \langle\beta^\dagger_{-\boldsymbol{k}}\beta_{-\boldsymbol{k}}\rangle$, and the polarization $P_{\boldsymbol{k}} = \langle\beta_{-\boldsymbol{k}}\alpha_{\boldsymbol{k}}\rangle$ are

$$\dot{f}^e_{\boldsymbol{k}} = \dot{f}^h_{\boldsymbol{k}} = 2\Omega(t)\sin\theta_{\boldsymbol{k}}\mathrm{Re}(P_{\boldsymbol{k}}) - \gamma_L f^{e/h}_{\boldsymbol{k}}, \tag{A2}$$

$$\begin{aligned} \dot{P}_{\boldsymbol{k}} = &-i\left[\varepsilon^e_{\boldsymbol{k}}(t) + \varepsilon^h_{\boldsymbol{k}}(t)\right]P_{\boldsymbol{k}} - \gamma_T P_{\boldsymbol{k}} \\ &+ \Omega(t)\sin\theta_{\boldsymbol{k}}\left(1 - f^e_{\boldsymbol{k}} - f^h_{\boldsymbol{k}}\right). \end{aligned} \tag{A3}$$

$\varepsilon^{e/h}_{\boldsymbol{k}}(t)$ is defined as $\varepsilon^{e/h}_{\boldsymbol{k}}(t) = E^{e/h}_{\boldsymbol{k}} + \Omega(t)\cos\theta_{\boldsymbol{k}}$. We have introduced relaxation terms to the above equation phenomenologically, as done in Sec. II. We define the macroscopic polarization of the system as the conjugate variable of the external field (light-matter coupling) as

$$\begin{aligned} p(t) &= \left\langle -\frac{\partial H}{\partial\Omega(t)} \right\rangle \\ &= \sum_{\boldsymbol{k}} \left\{ \cos\theta_{\boldsymbol{k}}\left(1 - f^e_{\boldsymbol{k}} - f^h_{\boldsymbol{k}}\right) - 2\sin\theta_{\boldsymbol{k}}\mathrm{Im}(y_{\boldsymbol{k}}) \right\}. \end{aligned} \tag{A4}$$

We consider the dispersion as $E^{e/h}_{\boldsymbol{k}} = \Delta/2 + \hbar^2\boldsymbol{k}^2/2m$ ($-\pi \leqslant k_x$, $k_y \leqslant \pi$), and an external field $\Omega(t) = \Omega_0 e^{-\frac{t^2}{\tau^2}}\cos(\omega_0 t)$. In this Appendix, the parameters are $m = 2.0$, $\gamma_\mathrm{L} = 2.0$, $\gamma_\mathrm{T} = 1.0$, and $\tau = 16.0\pi$, and we vary Δ, Ω_0, and ω_0. First, we show a typical HHG spectrum calculated for a semiconductor in Fig. 8. The spectrum shows a plateau and cutoff energy similar to two-level systems. Figure 9 shows the intensity of the $5\omega_0$ harmonics for various gap widths and Rabi frequencies. It becomes clear that for sufficiently large values of the Rabi frequency compared to the gap width, the intensity increases as the gap width is increased. The intensity of the $5\omega_0$ harmonics takes a maximum around $\Omega_0/\Delta \sim 7$. To confirm this behavior, we also show the gap dependence of the HHG at $\Omega_0 = 27.0$ in Fig. 10. The figure shows that the intensity increases

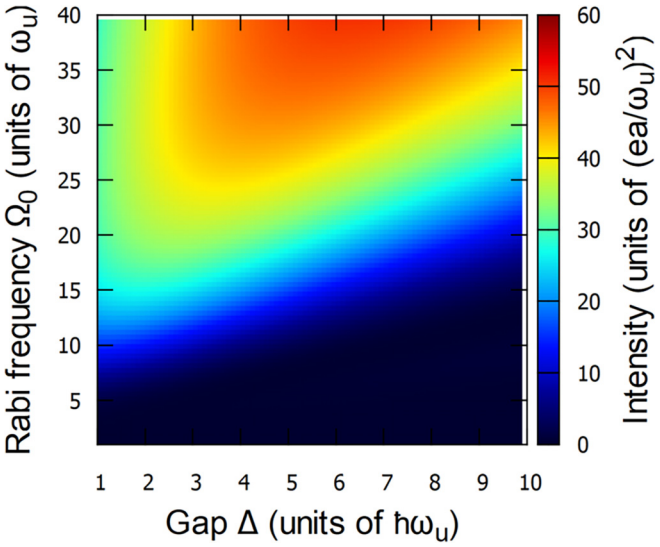

FIG. 9. Gap and Rabi frequency dependence of the 5th harmonics ($\omega = 5\omega_0$) in semiconductors. The incidental frequency is $\omega_0 = 0.3$.

until the gap width reaches some threshold and then decreases exponentially. Next, we show the enhancement ratio over the emission frequency $[|p(\omega; \Delta = 1.5)|^2/|p(\omega; \Delta = 1.0)|^2]$ for various incidental frequencies in Fig. 11. The incidental frequency is varied in the range $\omega_0 = 0.3 \sim 0.9$. The figure reveals that the enhancement ratio increases for increasing emission frequencies, demonstrating a universal scaling law that does not depend on the incidental frequency. We note that the enhancement ratio increases monotonically until $\omega = 7$ (except for $\omega_0 = 0.3$), contrary to the two-level system. This can be understood by considering the band dispersion, resulting in a momentum-dependent gap width. Semiconductors can partly be viewed as an ensemble of two-level systems with various gaps, which also include larger gaps compared to the minimum gap width Δ. As we have noted in Sec. III C, for larger gaps, the enhancement ratio holds even for higher emission frequencies. This explains the monotonic increase of the enhancement ratio in the case of semiconductors. Of course, this behavior is also parameter dependent similar to the case of two-level systems.

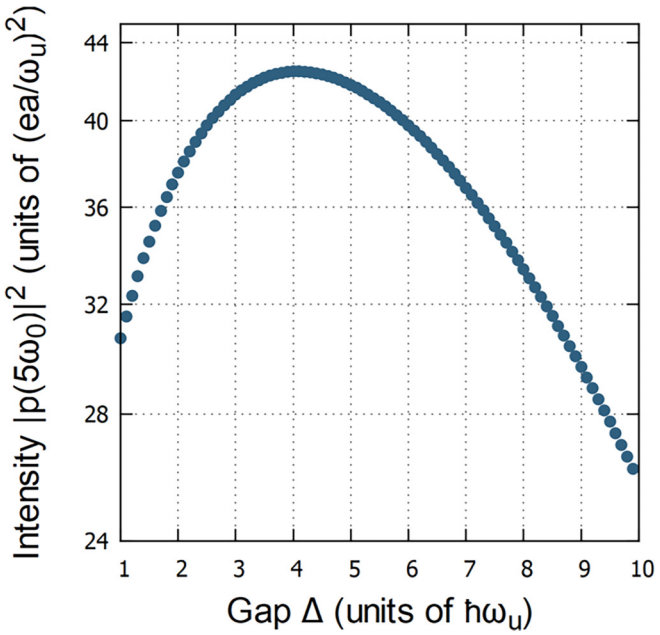

FIG. 10. Gap dependence of the 5th harmonics in semiconductors for $\Omega_0 = 27.0$. The incidental frequency is $\omega_0 = 0.3$. The vertical axis is log scale.

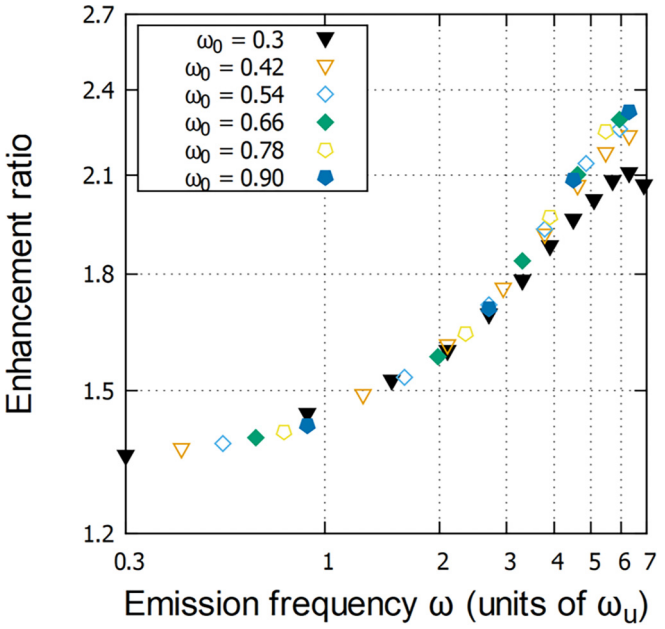

FIG. 11. Emission energy dependence of the enhancement ratio $|p(\omega; \Delta = 1.5)|^2/|p(\omega; \Delta = 1.0)|^2$ of the HHG in semiconductors. The Rabi frequency is $\Omega_0 = 22.7$. Both of the axes are log scale.

Thus, we conclude that when the Rabi frequency is sufficiently large compared to the gap width, HHG in semiconductors also shows an unconventional gap dependence similar to the two-level systems studied in the main text. This clearly shows that the origin of the unconventional gap dependence in the main text cannot be traced back to some particularity of two-level systems.

Finally, we comment on the momentum dependence of the Rabi frequency in Eq. (A1). The momentum dependence of the light-matter coupling is decided by the crystalline symmetry and the microscopic details of the system. It is known that they have crucial effects on the HHG [21,72,73]. For example, a momentum-dependent transition dipole moment increases the harmonic yields and the cutoff frequency significantly [73], and the anisotropy of the transition dipole moment directly leads to the anisotropy of the HHG [21]. However, in the experiment on the unconventional gap dependence of the HHG, they varied the intensity of the incidental laser field [39]. They did not find significant changes in the intensity dependence of the HHG. Thus, they concluded that the unconventional gap dependence of the HHG results from another origin other than the momentum dependence of the light-matter coupling. We also adopted this assumption and have shown one possible origin in this paper.

[1] A. McPherson, G. Gibson, H. Jara, U. Johann, T. S. Luk, I. A. McIntyre, K. Boyer, and C. K. Rhodes, Studies of multiphoton production of vacuum-ultraviolet radiation in the rare gases, J. Opt. Soc. Am. B **4**, 595 (1987).

[2] M. Ferray, A. L'Huillier, X. F. Li, L. A. Lompre, G. Mainfray, and C. Manus, Multiple-harmonic conversion of 1064 nm radiation in rare gases, J. Phys. B **21**, L31 (1988).

[3] F. Krausz and M. Ivanov, Attosecond physics, Rev. Mod. Phys. **81**, 163 (2009).

[4] S. Ghimire, A. D. DiChiara, E. Sistrunk, P. Agostini, L. F. DiMauro, and D. A. Reis, Observation of high-order harmonic generation in a bulk crystal, Nat. Phys. **7**, 138 (2011).

[5] S. Ghimire and D. A. Reis, High-harmonic generation from solids, Nat. Phys. **15**, 10 (2019).

[6] J. Itatani, J. Levesque, D. Zeidler, H. Niikura, H. Pépin, J.-C. Kieffer, P. B. Corkum, and D. M. Villeneuve, Tomographic imaging of molecular orbitals, Nature (London) **432**, 867 (2004).

[7] N. L. Wagner, A. Wüest, I. P. Christov, T. Popmintchev, X. Zhou, M. M. Murnane, and H. C. Kapteyn, Monitoring molecular dynamics using coherent electrons from high harmonic generation, Proc. Natl. Acad. Sci. USA **103**, 13279 (2006).

[8] S. Baker, J. S. Robinson, C. A. Haworth, H. Teng, R. A. Smith, C. C. Chirila, M. Lein, J. W. G. Tisch, and J. P. Marangos, Probing proton dynamics in molecules on an attosecond time scale, Science **312**, 424 (2006).

[9] S. Patchkovskii, Nuclear Dynamics in Polyatomic Molecules and High-Order Harmonic Generation, Phys. Rev. Lett. **102**, 253602 (2009).

[10] H. J. Wörner, J. B. Bertrand, B. Fabre, J. Higuet, H. Ruf, A. Dubrouil, S. Patchkovskii, M. Spanner, Y. Mairesse, V. Blanchet *et al.*, Conical intersection dynamics in NO_2 probed by homodyne high-harmonic spectroscopy, Science **334**, 208 (2011).

[11] A.-T. Le, T. Morishita, R. R. Lucchese, and C. D. Lin, Theory of High Harmonic Generation for Probing Time-Resolved Large-Amplitude Molecular Vibrations with Ultrashort Intense Lasers, Phys. Rev. Lett. **109**, 203004 (2012).

[12] G. Vampa, T. J. Hammond, N. Thiré, B. E. Schmidt, F. Légaré, C. R. McDonald, T. Brabec, D. D. Klug, and P. B. Corkum, All-Optical Reconstruction of Crystal Band Structure, Phys. Rev. Lett. **115**, 193603 (2015).

[13] T. T. Luu, M. Garg, S. Y. Kruchinin, A. Moulet, M. T. Hassan, and E. Goulielmakis, Extreme ultraviolet high-harmonic spectroscopy of solids, Nature (London) **521**, 498 (2015).

[14] M. Hohenleutner, F. Langer, O. Schubert, M. Knorr, U. Huttner, S. W. Koch, M. Kira, and R. Huber, Real-time observation of interfering crystal electrons in high-harmonic generation, Nature (London) **523**, 572 (2015).

[15] M. Lein, Attosecond Probing of Vibrational Dynamics with High-Harmonic Generation, Phys. Rev. Lett. **94**, 053004 (2005).

[16] Y. S. You, D. A. Reis, and S. Ghimire, Anisotropic high-harmonic generation in bulk crystals, Nat. Phys. **13**, 345 (2017).

[17] K. Kaneshima, Y. Shinohara, K. Takeuchi, N. Ishii, K. Imasaka, T. Kaji, S. Ashihara, K. L. Ishikawa, and J. Itatani, Polarization-Resolved Study of High Harmonics from Bulk Semiconductors, Phys. Rev. Lett. **120**, 243903 (2018).

[18] T. T. Luu and H. J. Wörner, Measurement of the Berry curvature of solids using high-harmonic spectroscopy, Nat. Commun. **9**, 916 (2018).

[19] H. Lakhotia, H. Y. Kim, M. Zhan, S. Hu, S. Meng, and E. Goulielmakis, Laser picoscopy of valence electrons in solids, Nature (London) **583**, 55 (2020).

[20] M. S. Mrudul, Á. Jiménez-Galán, M. Ivanov, and G. Dixit, Light-induced valleytronics in pristine graphene, Optica **8**, 422 (2021).

[21] K. Uchida, V. Pareek, K. Nagai, K. M. Dani, and K. Tanaka, Visualization of two-dimensional transition dipole moment texture in momentum space using high-harmonic generation spectroscopy, Phys. Rev. B **103**, L161406 (2021).

[22] M. R. Bionta, E. Haddad, A. Leblanc, V. Gruson, P. Lassonde, H. Ibrahim, J. Chaillou, N. Émond, M. R. Otto, Á. Jiménez-Galán, R. E. F. Silva, M. Ivanov, B. J. Siwick, M. Chaker, and F. Legare, Tracking ultrafast solid-state dynamics using high harmonic spectroscopy, Phys. Rev. Res. **3**, 023250 (2021).

[23] C. Heide, Y. Kobayashi, D. R. Baykusheva, D. Jain, J. A. Sobota, M. Hashimoto, P. S. Kirchmann, S. Oh, T. F. Heinz, D. A. Reis *et al.*, Probing topological phase transitions using high-harmonic generation, Nat. Photon. **16**, 620 (2022).

[24] G. Bae, Y. Kim, and J. Lee, Revealing Berry curvature of the unoccupied band in high harmonic generation, Phys. Rev. B **106**, 205422 (2022).

[25] N. Rana, M. S. Mrudul, D. Kartashov, M. Ivanov, and G. Dixit, High-harmonic spectroscopy of coherent lattice dynamics in graphene, Phys. Rev. B **106**, 064303 (2022).

[26] A. Pattanayak, S. Pujari, and G. Dixit, Role of Majorana fermions in high-harmonic generation from Kitaev chain, Sci. Rep. **12**, 6722 (2022).

[27] H. Liu, Y. Li, Y. S. You, S. Ghimire, T. F. Heinz, and D. A. Reis, High-harmonic generation from an atomically thin semiconductor, Nat. Phys. **13**, 262 (2017).

[28] R. E. F. Silva, I. V. Blinov, A. N. Rubtsov, O. Smirnova, and M. Ivanov, High-harmonic spectroscopy of ultrafast many-body dynamics in strongly correlated systems, Nat. Photon. **12**, 266 (2018).

[29] Y. Murakami, M. Eckstein, and P. Werner, High-Harmonic Generation in Mott Insulators, Phys. Rev. Lett. **121**, 057405 (2018).

[30] S. Takayoshi, Y. Murakami, and P. Werner, High-harmonic generation in quantum spin systems, Phys. Rev. B **99**, 184303 (2019).

[31] S. Imai, A. Ono, and S. Ishihara, High Harmonic Generation in a Correlated Electron System, Phys. Rev. Lett. **124**, 157404 (2020).

[32] M. Lysne, Y. Murakami, and P. Werner, Signatures of bosonic excitations in high-harmonic spectra of Mott insulators, Phys. Rev. B **101**, 195139 (2020).

[33] Y. Murakami, S. Takayoshi, A. Koga, and P. Werner, High-harmonic generation in one-dimensional Mott insulators, Phys. Rev. B **103**, 035110 (2021).

[34] W. Zhu, B. Fauseweh, A. Chacon, and J.-X. Zhu, Ultrafast laser-driven many-body dynamics and Kondo coherence collapse, Phys. Rev. B **103**, 224305 (2021).

[35] C. Orthodoxou, A. Zaïr, and G. H. Booth, High harmonic generation in two-dimensional Mott insulators, npj Quantum Mater. **6**, 76 (2021).

[36] C. Shao, H. Lu, X. Zhang, C. Yu, T. Tohyama, and R. Lu, High-Harmonic Generation Approaching the Quantum Critical Point of Strongly Correlated Systems, Phys. Rev. Lett. **128**, 047401 (2022).

[37] J. Alcalà, U. Bhattacharya, J. Biegert, M. Ciappina, U. Elu, T. Graß, P. T. Grochowski, M. Lewenstein, A. Palau, T. P. H. Sidiropoulos *et al.*, High-harmonic spectroscopy of quantum phase transitions in a high-Tc superconductor, Proc. Natl. Acad. Sci. USA **119**, e2207766119 (2022).

[38] T. Hansen, S. V. B. Jensen, and L. B. Madsen, Correlation effects in high-order harmonic generation from finite systems, Phys. Rev. A **105**, 053118 (2022).

[39] K. Uchida, G. Mattoni, S. Yonezawa, F. Nakamura, Y. Maeno, and K. Tanaka, High-Order Harmonic Generation and its Unconventional Scaling law in the Mott-Insulating Ca_2RuO_4, Phys. Rev. Lett. **128**, 127401 (2022).

[40] A. AlShafey, G. McCaul, Y.-M. Lu, X.-Y. Jia, S.-S. Gong, Z. Addison, D. I. Bondar, M. Randeria, and A. S. Landsman, Ultrafast laser-driven dynamics in metal-insulator interface, arXiv:2212.09176.

[41] A. Pizzi, A. Gorlach, N. Rivera, A. Nunnenkamp, and I. Kaminer, Light emission from strongly driven many-body systems, Nat. Phys. **19**, 551 (2023).

[42] K. S. Shimomura, K. Uchida, N. Nagai, S. Kusaba, and K. Tanaka, Ultrafast electron-electron scattering in metallic phase of 2H-$NbSe_2$ probed by high harmonic generation, arXiv:2302.04984v2.

[43] P. B. Corkum, Plasma Perspective on Strong Field Multiphoton Ionization, Phys. Rev. Lett. **71**, 1994 (1993).

[44] M. Lewenstein, P. Balcou, M. Y. Ivanov, A. L'Huillier, and P. B. Corkum, Theory of high-harmonic generation by low-frequency laser fields, Phys. Rev. A **49**, 2117 (1994).

[45] G. Vampa, C. R. McDonald, G. Orlando, P. B. Corkum, and T. Brabec, Semiclassical analysis of high harmonic generation in bulk crystals, Phys. Rev. B **91**, 064302 (2015).

[46] Mrudul M. S., A. Pattanayak, M. Ivanov, and G. Dixit, Direct numerical observation of real-space recollision in high-order harmonic generation from solids, Phys. Rev. A **100**, 043420 (2019).

[47] L. D. Landau, Zur theorie der energieubertragung, II, Phys. Z. Sowjetunion **2**, 46 (1932).

[48] C. Zener, Non-adiabatic crossing of energy levels, Proc. R. Soc. London, Ser. A **137**, 696 (1932).

[49] E. C. G. Stueckelberg, Theorie der unelastischen stösse zwischen atomen, Helv. Phys. Acta **5**, 369 (1932).

[50] E. Majorana, Atomi orientati in campo magnetico variabile, Nuovo Cimento **9**, 43 (1932).

[51] V. Ivakhnenko, S. N. Shevchenko, and F. Nori, Nonadiabatic Landau–Zener–Stückelberg–majorana transitions, dynamics, and interference, Phys. Rep. **995**, 1 (2023).

[52] L. V. Keldysh, The effect of a strong electric field on the optical properties of insulating crystals, Sov. Phys. JETP **7**, 788 (1958).

[53] L. V. Keldysh, Ionization in the field of a strong electromagnetic wave, Sov. Phys. JETP **20**, 1307 (1965).

[54] N. Yoshikawa, T. Tamaya, and K. Tanaka, High-harmonic generation in graphene enhanced by elliptically polarized light excitation, Science **356**, 736 (2017).

[55] N. Ishii, K. Kaneshima, K. Kitano, T. Kanai, S. Watanabe, and J. Itatani, Carrier-envelope phase-dependent high harmonic generation in the water window using few-cycle infrared pulses, Nat. Commun. **5**, 3331 (2014).

[56] Y. Murakami, K. Uchida, A. Koga, K. Tanaka, and P. Werner, Anomalous Temperature Dependence of High-Harmonic Generation in Mott Insulators, Phys. Rev. Lett. **129**, 157401 (2022).

[57] Y. Murakami and M. Schüler, Doping and gap size dependence of high-harmonic generation in graphene: Importance of consistent formulation of light-matter coupling, Phys. Rev. B **106**, 035204 (2022).

[58] A. E. Kaplan and P. L. Shkolnikov, Superdressed two-level atom: Very high harmonic generation and multiresonances, Phys. Rev. A **49**, 1275 (1994).

[59] V. P. Krainov and Z. S. Mulyukov, A plateau in high-order harmonic generation for a two-level atom, Laser Phys **4**, 544 (1994).

[60] F. I. Gauthey, B. M. Garraway, and P. L. Knight, High harmonic generation and periodic level crossings, Phys. Rev. A **56**, 3093 (1997).

[61] C. F. de Morisson Faria and I. Rotter, High-order harmonic generation in a driven two-level atom: Periodic level crossings and three-step processes, Phys. Rev. A **66**, 013402 (2002).

[62] P. Wei, Z. Guan, L.-L. Du, Z.-H. Jiao, L. Zhang, G.-L. Wang, S.-L. Hu, and S.-F. Zhao, Rabi-flopping signatures in below-threshold harmonic generation from the stretched H_2 and N_2 molecules in intense laser fields, Opt. Express **29**, 43212 (2021).

[63] R. W. Boyd, *Nonlinear Optics* (Academic Press, San Diego, 2020).

[64] B. Birnir, B. Galdrikian, R. Grauer, and M. Sherwin, Non-perturbative resonances in periodically driven quantum wells, Phys. Rev. B **47**, 6795 (1993).

[65] D. E. Nikonov, A. Imamoğlu, L. V. Butov, and H. Schmidt, Collective Intersubband Excitations in Quantum Wells: Coulomb Interaction versus Subband Dispersion, Phys. Rev. Lett. **79**, 4633 (1997).

[66] H. Kishida, H. Matsuzaki, H. Okamoto, T. Manabe, M. Yamashita, Y. Taguchi, and Y. Tokura, Gigantic optical nonlinearity in one-dimensional Mott–Hubbard insulators, Nature (London) **405**, 929 (2000).

[67] T. Ogasawara, M. Ashida, N. Motoyama, H. Eisaki, S. Uchida, Y. Tokura, H. Ghosh, A. Shukla, S. Mazumdar, and M. Kuwata-Gonokami, Ultrafast Optical Nonlinearity in the Quasi-One-Dimensional Mott Insulator Sr_2CuO_3, Phys. Rev. Lett. **85**, 2204 (2000).

[68] Y. Mizuno, K. Tsutsui, T. Tohyama, and S. Maekawa, Nonlinear optical response and spin-charge separation in one-dimensional Mott insulators, Phys. Rev. B **62**, R4769(R) (2000).

[69] G. P. Zhang, Origin of Giant Optical Nonlinearity in Charge-Transfer–Mott Insulators: A New Paradigm for Nonlinear Optics, Phys. Rev. Lett. **86**, 2086 (2001).

[70] T. S. Sarantseva, A. A. Silaev, A. A. Romanov, N. V. Vvedenskii, and M. V. Frolov, Time-frequency analysis of high harmonic generation using a probe XUV pulse, Opt. Express **29**, 1428 (2021).

[71] T. Tamaya, A. Ishikawa, T. Ogawa, and K. Tanaka, Diabatic Mechanisms of Higher-Order Harmonic Generation in Solid-State Materials under High-Intensity Electric Fields, Phys. Rev. Lett. **116**, 016601 (2016).

[72] Y. Qiao, J. Chen, and J. Chen, Review on the reconstruction of transition dipole moments by solid harmonic spectrum, Symmetry **14**, 2646 (2022).

[73] C. Yu, X. Zhang, S. Jiang, X. Cao, G. Yuan, T. Wu, L. Bai, and R. Lu, Dependence of high-order-harmonic generation on dipole moment in SiO_2 crystals, Phys. Rev. A **94**, 013846 (2016).